Composites Part C: Open Access 14 (2024) 100483

Contents lists available at ScienceDirect

Composites Part C: Open Access

journal homepage: www.sciencedirect.com/journal/composites-part-c-open-access

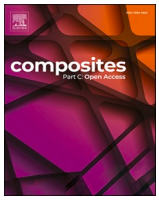

Engineering of a CMC aeronautical muffler

Marco Riva [a,*], Alessandro Airoldi [a], Marco Morandini [a], Rafał Żurawski [b], Lorenzo Cavalli [c], Matteo Boiocchi [c]

[a] Dipartimento di Scienze e Tecnologie Aerospaziali, Politecnico di Milano, Via La Masa, 34, 20156, Milan, Italy
[b] Łukasiewicz Research Network – Institute of Aviation, al. Krakowska 110/114, 02-256 Warsaw, Poland
[c] Petroceramics S.p.A., Viale Europa, 2, 24040 Stezzano (BG), Italy

ARTICLE INFO

Keywords:
Ceramic matrix composites
Composite structures
Mechanical properties
Oxidation resistance
Fabrication
Aerospace industry

ABSTRACT

This work explores the feasibility of adopting an LSI produced C/SiC composite to build an aeronautical Auxiliary Power Unit system muffler. The study first covers the experimental material characterization through tensile and compressive tests. The material properties are characterized also after exposing the samples to an oxidizing atmosphere, that is typical for the proposed application. The material response is characterized by significant non-linearities and a pseudo plastic response, which were numerically modeled using a Drucker-Prager model. The detailed design of the muffler is described and verified, for different loading conditions, using a Finite Element model. Finally, a full-scale prototype is produced and assembled, thus proving the technological feasibility of the design. The manufacturing phase required to study and understand the phenomena that were leading to defects in the proposed closed axial symmetric shape, and to implement suitable technological solutions in order to get an acceptable prototype.

1. Introduction

The environmental impact of the aeronautical compartment has been a primary focus in recent years. It was estimated that the sector CO_2 emission of 2018 where around seven times the one of 1960 [1]. Even though the COVID-19 pandemic significantly impacted the sector, with a reduction of revenue passenger kilometers of 50 % by mid-2020 [2], the sector was predicted to recover between 2022 and 2026 [3] and already by mid-2022 some players of the sector were outperforming their pre-pandemic records, indicating that, even if globally the system is below the pre-pandemic level, the recovery is ongoing [4]. Considering the pre-pandemic grow trends, the sector will not meet the required emission reduction for decarbonization goals [2]. The possible strategies to mitigate the environmental impact are various; among them, the implementation of new technologies [5]. This work focused on the development and implementation of new material construction concepts to optimize the Auxiliary Power Unit (APU) exhaust muffler, aiming to increase the efficiency of the whole system. Aircraft APU are gas generators that are used to provide power to the aircraft when main engines are shut down, thus saving fuel during ground operations. Depending on the aircraft configuration the APU is used to power electric, hydraulic, pneumatic systems and to act as a starter for the main engines, saving the weight of an equivalent electric system. Moreover, the APU is used to provide backup in emergency conditions, and, for these reasons, the APU is required to be compact, fuel efficient, lightweight, reliable, silent and of easy maintenance and operation, as most of the aeronautical critical component are required to be [6]. The APU system requires different supporting components to perform its task; an air intake, an exhaust muffler and a fuel supply line are mandatory. Exhaust mufflers not only bring the exhaust gas outside the aircraft, but also reduce the emitted noise. In this regard, mufflers are classified, based on the working principle, as active or passive. The passive ones can be further separated into dissipative or reactive, and the second category is the most used to attenuate noise of engines [7]. For the proposed application, a reactive muffler is designed by taking, as a starting point, the current solution, which is based on two coaxial metallic tubes connected using baffles. By changing the material from metallic to a ceramic matrix composite, the new redesigned muffler should outperform the predecessor, especially in terms of reduced weight, a fundamental objective for aerospace applications.

The proposed solution substitutes the metallic material with a Carbon/Silicon Carbide (C/SiC) Ceramic Matrix Composite (CMC) produced via Liquid Silicon Infiltration (LSI). CMC were originally developed for high temperature applications and were produced using

* Corresponding author.
E-mail address: marco2.riva@polimi.it (M. Riva).

https://doi.org/10.1016/j.jcomc.2024.100483

Available online 21 June 2024

long and costly procedures. The LSI technique was developed at DLR in 2001 [8] and consists in the infiltration of molten silicon into a porous carbon preform. The process allowed to reduce the cost and the time of production, paving the way for the application of the material into different fields of mechanical engineering [9]. The microstructure of the material is characterized by a dense network of microcracks which is formed during the pyrolysis and cooldown phase of the manufacturing [10,11] and which acts as crack stopper. Moreover, the weak fiber matrix interface combines the typical bulk ceramic properties with a reduced brittleness and increased damage tolerance, leading to a material with a more ductile behavior than that of monolithic ceramic [12, 13].

One of the main drawbacks of C/SiC is the intrinsically oxidation prone nature of the constituents, that when exposed to oxygen can lead to an active oxidation, as from C to CO or CO_2 and from SiC to CO and SiO, or to a passive oxidation, as for SiC to SiO_2 [14,15]. The active oxidation is particularly critical for the material, since it leads to the release of a gaseous product and a mass loss which, in turn, leads to a reduction of the mechanical properties. On the contrary, passive oxidation leads to the creation of a layer of oxide protecting the underlying material. These oxidation phenomena are investigated in the literature [14–17] and, depending on the temperature at which the component is subjected, can be divided into three mechanisms. For temperatures lower than 800 °C the resulting degradation is uniformly distributed into the material. The thermal expansion of the matrix is not sufficient to close the process-induced microcracks and the oxygen is able to reach the carbon fibers. The carbon reactivity is slow, and the oxygen diffuses in the cracks and attacks the carbon fibers uniformly in the specimen, while the passive oxidation of the matrix is negligible due to its slow kinetic. At intermediate temperatures, up to 1000 °C, the SiC matrix expansion partially closes the microcracks and the reaction kinetic of the fibers oxidation is increased. This leads to an increased oxygen consumption by the external carbon fibers, which results in a non-uniform degradation. Finally, at high temperatures the SiC matrix expansion closes almost completely the microcracks while both the oxidation kinetic of the matrix and of the fibers becomes relevant. This leads to an initial fast degradation of the outer tows, which stops as soon as the silica layers forming on the microcrack walls occludes completely the microcracks, creating a passive layer protecting the material. The latter mechanism leads to a superficial degradation of the matrix, which is less aggressive on the mechanical properties of the material. The reduction of oxidation effects at high temperatures was not observed on short fibers reinforced composites, since the oxidation phenomena is regulated by the short fibers network disposition and contact, while the microcracking closure effect is negligible [18,19]. Some possible actions to alleviate the damage can be found in literature, such as coating application or microstructure tailoring [17,20].

This work aims to design a modular solution for an aeronautical muffler adopting a CMC material, which microstructure was designed to be able to survive in an oxidizing environment. The usage of a modular solution will increase the repairability of the muffler and the manuscript will outline the main technological aspects of the manufacturing process. The work is divided into five sections, including the present introduction. The second section introduces the specific problem investigated, highlighting the innovative concepts of the solution. Section three reports the results of the material characterization campaign performed and discusses the identified material characteristics. The fourth section illustrates the detailed design and the numerical verification of the design itself, based on the results obtained in section three. Moreover, a material model to be employed in FEM analyses is presented. Finally, section five delineates the manufacturing of the technological demonstrator, focusing mainly on the definition of the layup and the lamination of the polymeric precursor.

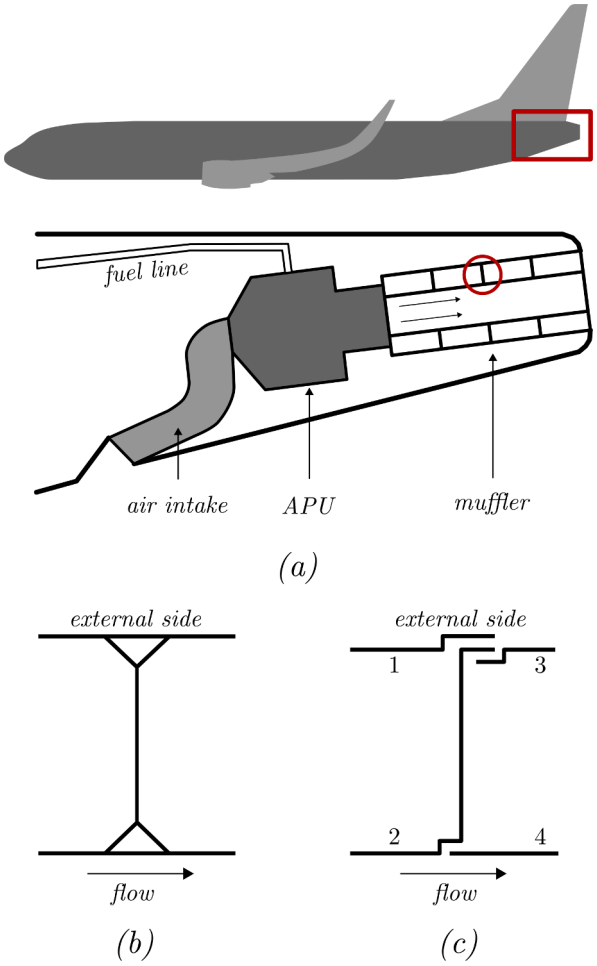

Fig. 1. (a) schematic drawing of the location of the APU and correlated systems in the aircraft tail cone. The circle on the sectioned muffler highlights the connection of the coaxial tubes reported in subfigure (b) current configuration of the connection and subfigure (c) proposed modular connection.

2. Design problem and innovative concepts

The work presented in this paper aims to improve the efficiency of an aircraft APU system by upgrading the design of the exhaust muffler. Fig. 1a reports an exemplifying scheme of the positioning of the APU and its support components with respect to the aircraft. A complete redesign of the component was avoided to reduce compatibility issues with the power generator and the other parts housed in the tail cone compartment. As presented in the introduction, the current solution makes use of two coaxial tubes with internal baffles and an external heat blanket increases the muffler thermal insultation. Fig 1b presents a simplified drawing of the joining between the tubes and the baffles. The new solution was required to achieve a lower weigh and to reduce the emitted noise, while at the same time providing at least the same thermal insulation, fire resistance, fluid drainage and survivability in the environmental working conditions. To comply with all the requirements, the introduction of an LSI (Liquid Silicon Infiltration) produced C/SiC ceramics matrix composite (CMC) as a substitute to the metallic material was mainly intended to reduce the global weight of the muffler. In fact, for the proposed application temperature range, a typical alloy for high temperatures, namely the Inconel 718, has a Young Modulus between 150 and 165 GPa and a tensile strength that exceeds 800 MPa. While the former property is comparable with the CMC, the latter cannot be matched by the composite material. However, the proposed application is not a structural one, thus the strength disadvantage is not crucial.

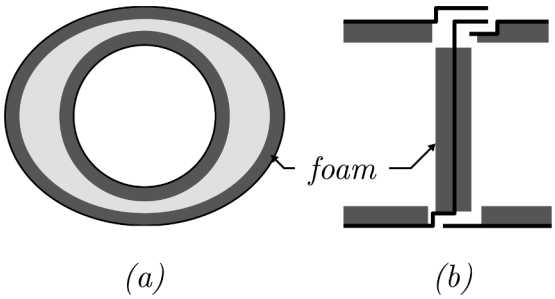

Fig. 2. (a) axial section with proposed foam application region, (b) transversal section with foam application.

Furthermore, the Inconel and CMC materials have significantly different densities: while the Inconel density is around 8.0 g/cm^3, the CMC density is comparable with the one of aluminum alloys (2.7 g/cm^3) [21]. Moreover, the usage of CMC allows the removal of the heat blanket, due to a lower thermal conductivity, further reducing the global weight of the muffler, still guaranteeing the required fire and fluids resistance. Although the LSI technique leads to substantial reduction of costs in CMC production, the overall cost of a single CMC muffler is expected be higher than that of the current metallic solution, due to both higher raw material costs and manufacturing costs; however, the predicted performance improvement should more than balance the increased costs.

The basic solution for noise abatement of the muffler was maintained, using two coaxial tubes with internal chambers separated by baffles, but a minor redesign allowed to adopt a modular solution as shown in the sketch of Fig. 1c.

The modular configuration grants the possibility to separate the different parts of the muffler, and, consequently, to simplify the inspection and substitution of damaged parts, hence reducing maintenance costs. Referring to the identification numbers of Fig. 1c, the modular solution will require the assembly of the components in ascending order, repeating the procedure for each chamber. The axial section view of Fig. 2a shows that the proposed cross-section is elliptical, while the current solution has a circular cross-section. The elliptical cross-section, while ensuring compatibility with the existing mounting points on the shorter axis, allowed to improve the noise attenuation performance of the component, by both increasing the volume of the resonating chamber and leveraging the intrinsic higher attenuation of elliptical shapes [7].

The usage of LSI technique and C/SiC composite gave the possibility to manufacture, by simultaneous infiltration, a layer of SiSiC ceramic foam. This possibility was exploited to increase the noise abatement capability of the muffler. The optimal solution would have been to completely fill the external chamber with foam. However, the maximum manufacturable foam thickness is limited. Furthermore, the thermal conductivity of SiSiC foam ceramic would have led to a higher temperature on the external surface with respect to a solution presenting void cavities. For these reasons, the chosen foam thickness represents a tradeoff between the desired noise attenuation, thermal insultation and technological considerations. Fig. 2 clarifies where the foam was applied. Currently, the muffler and heat blanket assembly weights about 34 kg, while the proposed solution in CMC with foam layers weights a little more than 26 kg, presenting a weight reduction of more than 20 %.

3. Characterization of material response

The selected material is produced via LSI by Petroceramics S.p.A with an internal structure consisting of a 1 × 1 twill carbon reinforcement in a silicon carbide matrix. A SEM image of a typical as built material section is reported in Fig 3. The material is characterized by a density of 2.35 g/cm^3 and an open porosity of about 1.5 %. The main constituents weight ratio is between 47 % and 53 % for SiC and between 44 % and 45 % for C. The material presents a residual silicon component between 1 % and 5 % in weight ratio. This material is designed to sustain oxidation better than other LSI counterparts.

Mechanical tests performed on the material allowed to verify its suitability for the application at hand. The scope of the tests was to evaluate the material mechanical properties and the allowable stresses, and to prove the material capability to survive in an oxidizing atmosphere at relatively low temperature for a long time. In detail, the material was tested in:

- Traction, with two lamination sequence [0°]and [45°], to evaluate the elastic and shear modulus and the relative strengths.
- Compression, using only the [0°] layup, to investigate eventual differences between the traction and compression behavior and to evaluate the compressive strength of the material.

The proposed application required the capability to sustain temperatures of around 600 °C for long periods of times, in the order of thousands of hours, in a dry air. For this reason, a subset of specimens for each type of test was kept at 650 °C in dry air for 250 h, matching the expected real-life operation of the muffler. After the treatment the

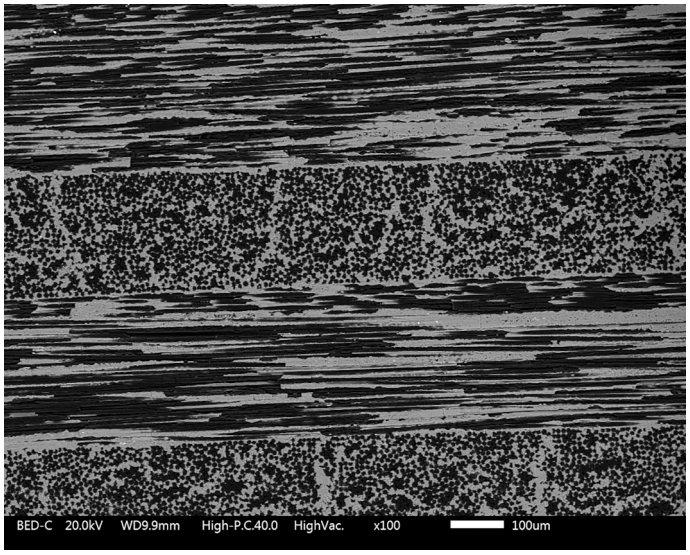

Fig. 3. SEM image of an as built material section.

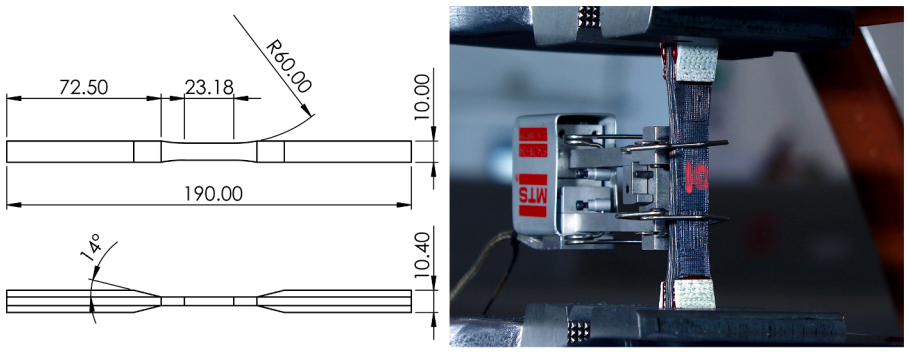

Fig. 4. (a) Tensile specimen geometry and (b) example of specimen under testing.

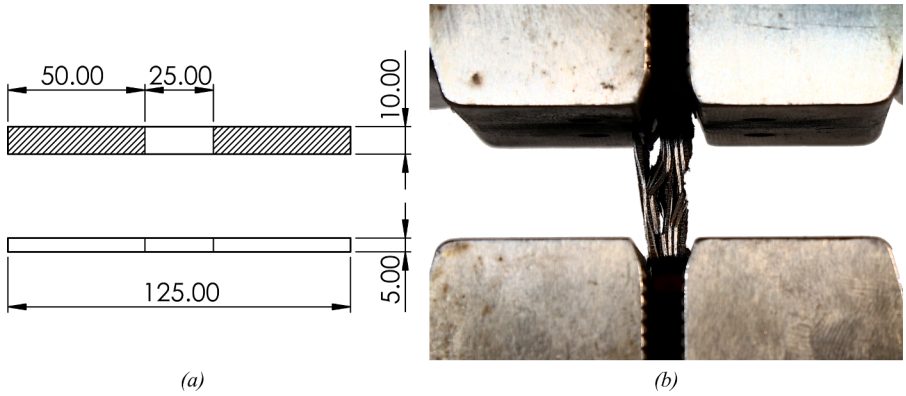

Fig. 5. (a) Compressive specimen geometry and (b) typical failure observed in the compression tests.

specimens presented a weight loss of about 6% due to oxidation.

3.1. Experimental campaign design

As said in the introduction to this section, the material was tested in traction and in compression. The tensile tests were performed on 20 specimens, equally divided between [0°] and [45°] layups. For each set half of the specimens were subjected to the oxidizing treatment. The test procedure was set up according to the standard ASTM C1275 [22], which provides a reference for the monotonic tensile test of ceramic matrix composites. The specimens were cut using waterjet from two plates, one of which was previously subjected to the oxidation cycle. The dog bone shape and dimensions of the specimen are reported in Fig. 4a. Additionally, Fig. 4a reports the dimensions of the tabs applied to the specimens using the secondary bonding technique, in which the two pre-cured laminates are joined by curing a layer of epoxy-based structural adhesive between them, specifically Scotch Weld AFK 163–2 K. These tabs were obtained by machining a uniform plate of $[45°]_{10}$ Glass/Epoxy fabric reinforced composite. The testing machine used was an MTS 810 material testing system. A constant head displacement velocity of 0.5 mm/min was prescribed, while measuring the applied force and the strain; an extensometer MTS 634.31F-24 with 20 mm of gage length placed at the center of the specimen was used for the strain measurement. The testing configuration is reported in Fig. 4b. For all the specimens unloading and reloading cycles were performed during the test, which was stopped at the failure of the specimen.

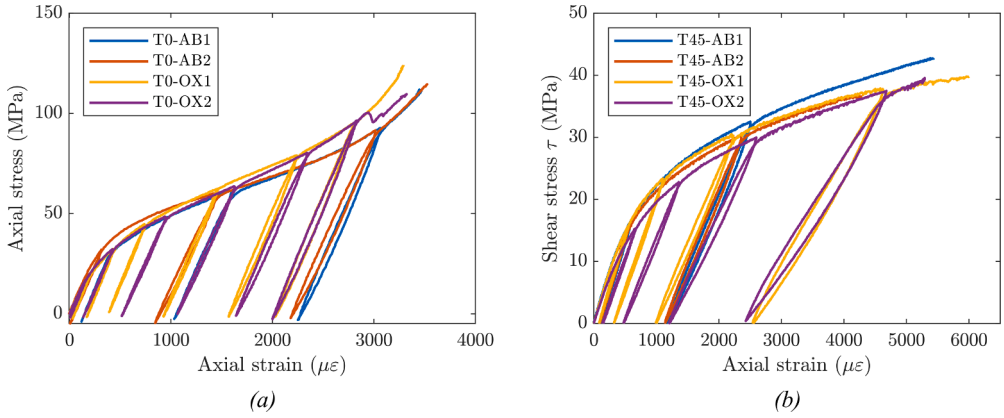

Fig. 6. (a) Axial stress versus axial strain response of four representative [0°] specimens and (b) shear stress versus axial strain response of four representative [45°] specimens.

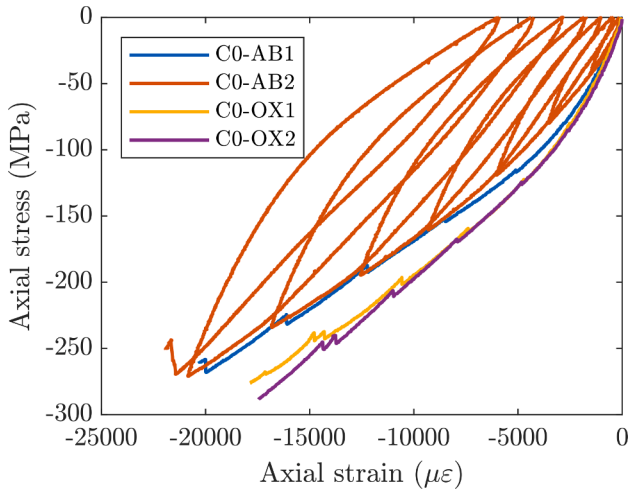

Fig. 7. Stress strain response of four representative specimens for compression tests.

Table 1
Summary of the identified properties during the experimental testing campaign.

		As built		Oxidized @ 650 °C for 250 *h*	
		Mean value	Std deviation	Mean value	Std deviation
Traction at [0°]	E (GPa)	117.8	8.8	107.0	7.2
	σ_f (MPa)	114.0	5.8	108.0	17.0
	ε_f (με)	3617	114	3361	96
Traction at [45°]	G (GPa)	28.0	4.3	-	-
	σ_f (MPa)	37.0	3.6	37.8	2.5
	ε_f (με)	4765	821	5145	650
Compression at [0°]	E (GPa)	40.0	2.8	51.2	4.7
	σ_f (MPa)	-250.8	32.5	-263.2	25.1
	ε_f (με)	-20,587	3096	-17,571	1406

For the test of the [45°] layup, in addition to the extensometer, a rosette strain gauge was installed with the two normal strain gages aligned with the specimen longitudinal (subscript *x*) and transverse axis (subscript *y*), respectively; this allows to evaluate the shear modulus of the material by computing the slope of the first part of the τ_{12} - γ_{12} response, where the subscript 1 and 2 are referred to material axis. The shear stress (τ_{12}) was evaluated as half the axial stress σ_x, while the shear deformation was computed as $\gamma_{12} = \varepsilon_x$ - ε_y, measured by the two normal strain gages of the rosette. This procedure follows the one prescribed by the standard ASTM D3518 for the evaluation of shear modulus by tensile tests of polymeric matrix composite materials [23].

The compression tests were performed on eleven [0°] specimens, five of which were kept as built and six were subjected to oxidation. The specimens were cut from two plates following the dimensions prescribed by the standard ASTM C1358 [24]; their geometry is reported in Fig. 5a. Differently from the tensile test the standard does not prescribe the usage of tabs for this type of test and, due to the short dimension of the gage length, the specimens were not instrumented. Both the applied force and displacement were directly measured from the MTS 810 testing machine. A constant velocity of -0.5 mm/min was prescribed. During the test the specimens were subjected to loading unloading cycles and the test was carried on up until failure. Fig. 5b shows the typical brooming failure mode, which is driven by the local buckling of the plies.

3.2. Results of the experimental campaign

The results of the experimental campaign are reported in this subsection, where exemplifying responses are shown. Starting from the tensile tests, Fig. 6a reports the axial stress strain response of two as built (T0-AB*k*) and two oxidized (T0-OX*k*) representative specimens during a tensile test with layup [0°]. The behavior of the material is characterized by a pseudo plastic response, which can be identified by the parallel loading unloading cycles. The response is composed by three regions, a first, short, elastic region, as the material response is nonlinear almost from the beginning, followed by a longer region where an apparent reduction of the tangential modulus can be seen and where the pseudo plasticity is highlighted by the loading and unloading cycles. Finally, there is a short region where the material seems to regain its stiffness, followed by the failure of the specimen. In literature some authors reported the correlation between Residual Thermal Stresses, fiber matrix sliding, matrix microcracking, and the nonlinear material behavior [12, 25–27]. Shi et al. in [28] showed that the non-linearities disappear when the material is tested at high temperatures. The possible relation between nonlinear response and RTS was proposed by Galizia and Sciti in [29] and was formalized by Caporale et al. in [30] associating it to damage evolution in the material. A more accurate investigation of the root causes of this phenomenon goes beyond the scope of this work.

Fig. 6b shows the response, in terms of shear stress (τ_{12}) and axial strain (ε_x) of the [45°] layup, which was characterized, as for the [0°] layup, by pseudoplasticity. After the first part of the response where the material showed a pseudoplastic response, the loading unloading cycles were also showing indication of damages, as can be identified by the reduction of the tangential elastic modulus of the unloading and loading cycles. This can be attributed to the fact that the [45°] response is dominated by the matrix properties, rather than by the fiber properties. In both testing cases the oxidation effects on the specimen responses can be neglected, in fact both Fig. 6a and b report similar response and strength for the representative as built and oxidized response.

For the compressive tests, four exemplifying responses are reported in Fig. 7. The compressive response was characterized by two regions, a first short linear elastic region and a second longer and less stiff region, that is maintained until failure. The loading unloading cycles, reported only for specimen C0-AB2, were characterized by a noticeable hysteresis. During both the loading and the unloading phase, the tangent stiffness was initially similar to the initial stiffness of the test and then it decreased to reach comparable values with the apparent stiffness of the second phase of the loading-only curve. This hysteresis tends to grow as the strain increases. A different behavior is shown by the as built and the oxidized material, with the latter failing at lower strain but at comparable stresses, probably because of the thermal treatment. The authors recognize that this phenomenon is quite peculiar and worthy of an exhaustive study, which goes beyond the scope of this work and could be a topic for future works. At any rate, this difference is negligible from an engineering point of view, especially at the relatively low strain values predicted for the application at hand.

A summary of the identified properties for the material is reported in Table 1, where the different behavior in traction and in compression is easily identifiable. The compressive tests show a reduction of two thirds of stiffness but a failure strength and strain which are two and five times the one identified in traction, respectively. The scattering of the properties measured experimentally is noticeable and the discrepancy between oxidized and as built properties are compatible with the test results standard deviation. For this reason, the authors believe that the tests demonstrate that the material can be used in oxidizing conditions, without initiation of significant damages. Finally, the testing highlighted the presence of a pseudoplastic response, showing that the material can sustain noticeable deformations before reaching the failure point.

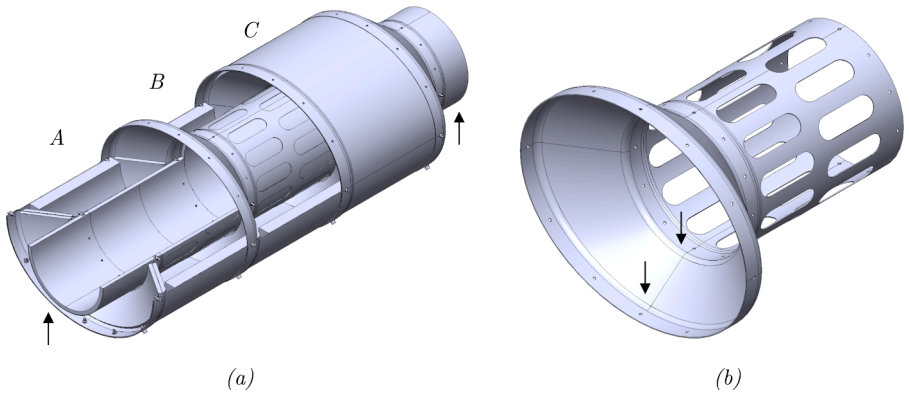

Fig. 8. 3D model of the part: (a) full assembly with different degrees of sectioning, (b) internal part.

4. Design and verification

This section covers the detailed design of the muffler, which implements the ideas shown in Section 2 and account for technological consideration. The design was subjected to a numerical verification using a detailed Finite Element model, to ensure that the prescribed operative condition can be sustained by the muffler.

4.1. Detailed design of the muffler

The detailed design required to consider the technological aspects of the manufacturing of a doubly symmetric shape with double curvature regions in CFRP, which poses issues on the feasibility of the lamination phase [31,32]. In addition, the material choice was driven by resistance to oxidation rather than by drapability. As a matter of fact, the 1 × 1 twill with a tow size of 5 mm significantly complicates the lamination process. It was decided to use ample radii for the fillets and to incline the baffles by 45° aiming to simplify the lamination. It was further decided to keep at a minimum the required number of internal parts, which were deemed the most technologically complex, thus reducing the number of baffles with respect to the current solution. While the internal part was obtained by a single axial-symmetric part, it was decided to obtain the external parts by secondary bonding of two identical halves, thus avoiding the introduction of a closed axial symmetric section. Due to the complex shape and the expected low mechanical loads, it was decided to adopt a layup of [0°/45°/0°] for the whole component, allowing to have flexibility in the definition of the ply cutting shapes, which was a fundamental step to define a good lamination procedure.

The final assembly, reported sectioned in Fig. 8a, was composed of eleven parts, with four basic parts. Three of the basic parts were obtained from the same mold, namely the internal part mold: the full internal part and two halves of it, which will be used as inlet and outlet of the muffler highlighted in Fig. 8a with the arrows. Moreover, the figures report a fully sectioned sector (A), a sector with removed external parts (B) and a closed sector (C), the latter representative of the final assembly aspect. Fig. 8b reports the isolated internal part, with the arrows pointing to the double curvature region. Moreover, the figure illustrates some holes introduced in the design aiming to improve noise attenuation; these holes were obtained by machining after pyrolysis.

By design the different parts were joined using screw acting on floating nuts or bolts. The usage of floating nuts was forced by the unfeasibility to access to the chambers during the assembly phase, which followed the order shown in Fig. 1c. As said in Section 2 the maximum foam thickness was limited and represented a compromise between technological limitations and noise attenuation performance.

4.2. Finite element model set up

The proposed design was verified by means of a FE model of the whole assembly, subjected to four representative loading conditions. The loading conditions consist in a combination of inertial loads, temperature, and pressure. The loads are reported as normalized values in Table 2. The solutions were obtained with four different simulations, all of which with null initial pressure, acceleration, and temperature. The pressure was applied to the external case, with positive direction in the outward radial direction. The accelerations were applied to all the elements, with, taking as reference the axis of Fig. 10, axial directed as x and planar directed as y. Finally, the internal temperature was applied on the internal tube and the external temperature to the external casing. The external constraints were applied to four reference nodes; rigid body replaced the brackets acting on the external casing in the reality, and the constraints were set up so to allow stress-free thermal expansion of the muffler, as in the real case.

Table 2
Load cases definition.

Load case	Pressure	Inertial load	Internal temperature	External temperature
Positive pressure	0.87 P	-	0.91 T	0.45 T
Negative Pressure	-P	-	0.91 T	0.45 T
Axial inertial load	-	0.79 a	T	0.25 T
Planar inertial load	-	a	T	0.25 T

The detailed Finite Element (FE) model required the definition of a material model able to represent the pseudo-plastic response identified during the experimental testing. Due to asymmetry in traction and compression it was decided to represent the material behavior using a Drucker-Prager model with associated flows, which is already implemented in Simulia/Abaqus [33] and is a common solution in literature [30,34,35]. The muffler is a nonstructural component, having to sustain just its own mass forces. For this reason, it was not expected to be subjected to high deformation and a tuning of the model over the interval from -3000 με to 3000 με was considered acceptable. The result of the tuning is reported in Fig. 9a, where the experimental response is compared with the numerical one. The hardening has a tabular definition based on the tensile response, as can be seen by the perfect numerical experimental correlation in traction, while the material elastic characteristics and the angle of friction are reported in Table 3.

In compression the model overestimates the stiffness in the first part of the response, up to around -1500 με. Fig. 9b compares the experimental response of the material at 45° and the numerical response shows that the model departs from the experimental curve at around 1000 με. The material model correlation was considered acceptable to represent the material behavior in the FEM, since the component was not expected to sustain high loads and because this simplified model would have

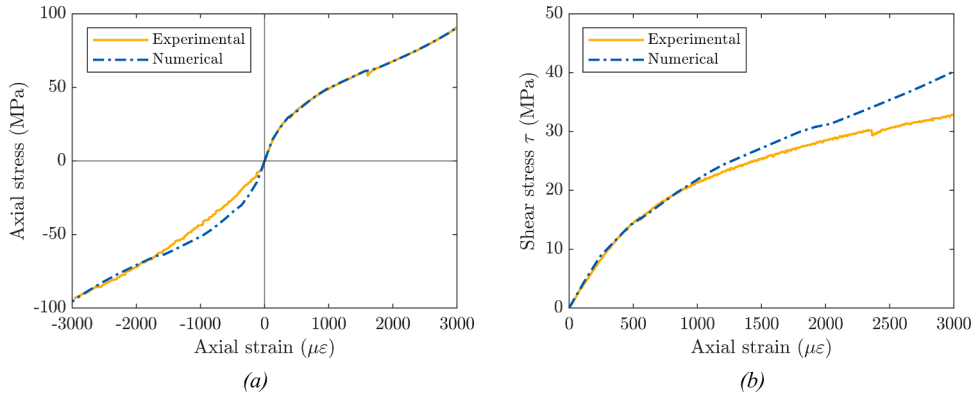

Fig. 9. Numerical experimental correlation of the Drucker-Prager material model for (a) traction and compression at 0° and (b) for traction at 45°.

Table 3
Drucker-Prager material model properties.

E_{11}	120,000 MPa
E_{22}	120,000 MPa
E_{33}	20,000 MPa
ν_{12}	0.01
ν_{13}	0.30
ν_{23}	0.30
G_{12}	27,500 MPa
G_{13}	12,000 MPa
G_{23}	12,000 MPa
σ_y	16.27 MPa
β	3.13°

highlighted any issue for which further investigations would have been necessary. Finally, to account for thermal deformations, a tabular definition of the thermal expansion coefficients, which were obtained in previous experiments, was added to the material model.

An isotropic material was used for the SiSiC foam, with $E = 4000$ MPa and $\nu = 0.01$. The simulation was performed using Abaqus/Standard. It was decided to avoid the modeling of the discrete junctions; rather, a tie constraint over the whole contact faces was used [33]. The whole model was composed by more than 2.6 million elements, of which about 140 thousand were SC8R, eight nodes continuum shells [33], and 2460 thousand where C3D10, quadratic tetrahedral elements [33]. The continuum shells were used to model the parts in CMC, reducing the number of elements required with respect to those that would have been required with a solid-based model, while the tetrahedral elements were used to mesh the foam, which presented complex shapes. The meshes were joined by resorting to tie constraints between the parts.

4.3. Results of the numerical verification

The main interest of the simulation was to evaluate the state of stress in the composite since the foam do not have a structural role. Between the four conditions tested, similar results were obtained by comparing the two pressure loads between them and by comparing the two inertial loads. This led to assume that the main driver of the stress status was the thermal load and the consequent mismatch of expansion between the internal and external part, rather than the pressure or the inertial loads. Fig. 10a reports the contour of the stress component σ_{11} in a 0° ply while the assembly was subjected to axial inertial load, which was the most critical condition. For the same load case the maximum stresses found in the different plies are reported in Table 4. From the table it can be seen that the stresses, if compared with Fig. 9, are close to the start of the non-

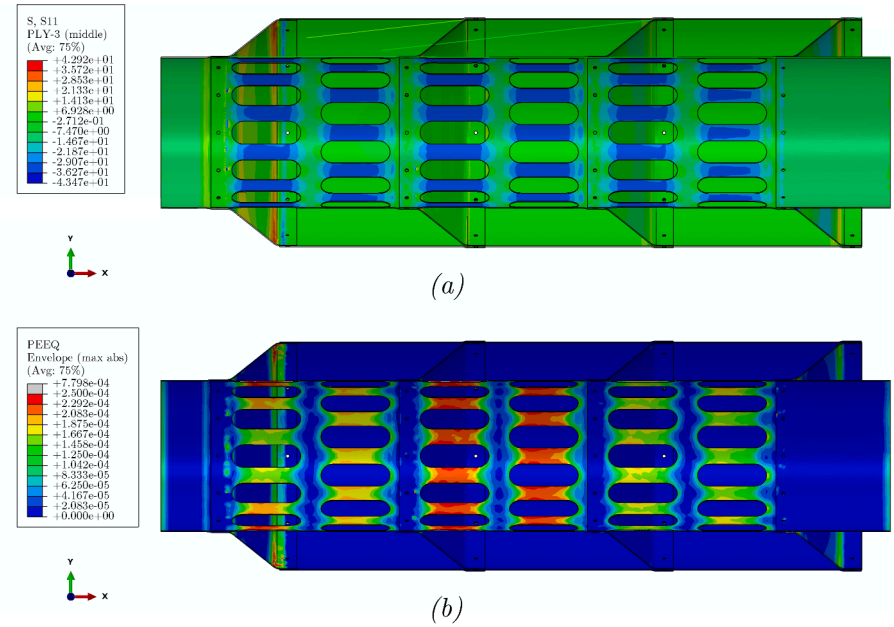

Fig. 10. Different contours of the FEM results while subjected to axial inertial load: (a) distribution of stress σ_{11} in a 0° ply, (b) distribution of maximum PEEQ in the thickness with scale limited to 250 με.

Table 4
Peak stresses and maximum PEEQ evaluated in the plies for axial inertial loading condition.

Ply	σ_{11}^{trac} (MPa)	σ_{11}^{comp} (MPa)	σ_{22}^{trac} (MPa)	σ_{22}^{comp} (MPa)	τ_{12} (MPa)	PEEQ (με)
0°	42.7	-51.8	22.9	-40.5	9.9	780
45°	17.7	-31.5	18.1	-31.5	12.0	176
0°	42.9	-43.6	20.6	-33.6	13.3	563

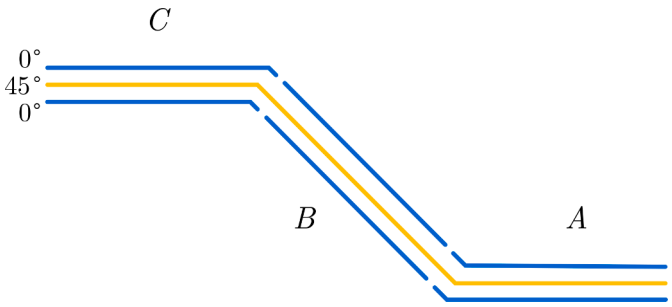

Fig. 11. Axial section with ply separation (sketch not in scale).

linearity and far from the failure points. Moreover, the table reports the peak equivalent plastic strain (PEEQ) evaluated in the muffler. The values obtained are noticeable, but it should be noted that most of the muffler stays well below the 250 με, as reported in Fig. 10b where the contour is limited to 250 με. In addition, it should be remembered that the nonlinearity of the response is fully attributed to plasticity, requiring to adopt a yielding stress for the criterion of $\sigma_y = 16.27$ MPa, which is a relatively low value.

In conclusion, the FE model indicated that the design should be able to sustain the required loads, being the material stress state far from failure. It should be noted that the stress concentration in the discrete junctions cannot be represented by the implemented model. Due to the material pseudo-plastic behavior and a low "yielding" stress, the assembly will always operate at the nominal elastic modulus with a small, with respect to the whole muffler length, plastic deformation, as indicated by the non-zero PEEQ.

5. Technological demonstrator manufacturing

The internal part was considered the most complex part to be manufactured; for this reason it was decided to concentrate the main technological trials over its production, considering that the external parts could be easily obtained. Since the parameters for the pyrolysis and infiltration phases of the LSI technique were fixed, the focus was posed on the manufacturing of the CFRP, aiming to reproduce the complex shape required still respecting the dimensional tolerances and ensuring the different part compatibility for the subsequent assembly phase.

5.1. Layup design

The designed layup was composed by three plies, considering the resulting thickness sufficient to meet the structural and thermal requirements. The orientation was selected mainly based on technological considerations and, taking as reference direction the axis of the muffler, it was oriented as [0°/45°/0°]. The 45° drapability was intended to provide continuity to the layup, since, in the axial direction, it would not have required discontinuity to be adapted to the shape, while the 0° required some separation to be deposed on the shape. The ply separation position is reported in the schematic drawing of Fig. 11, where the continuity of the 45° and the separation in the 0° plies are made evident.

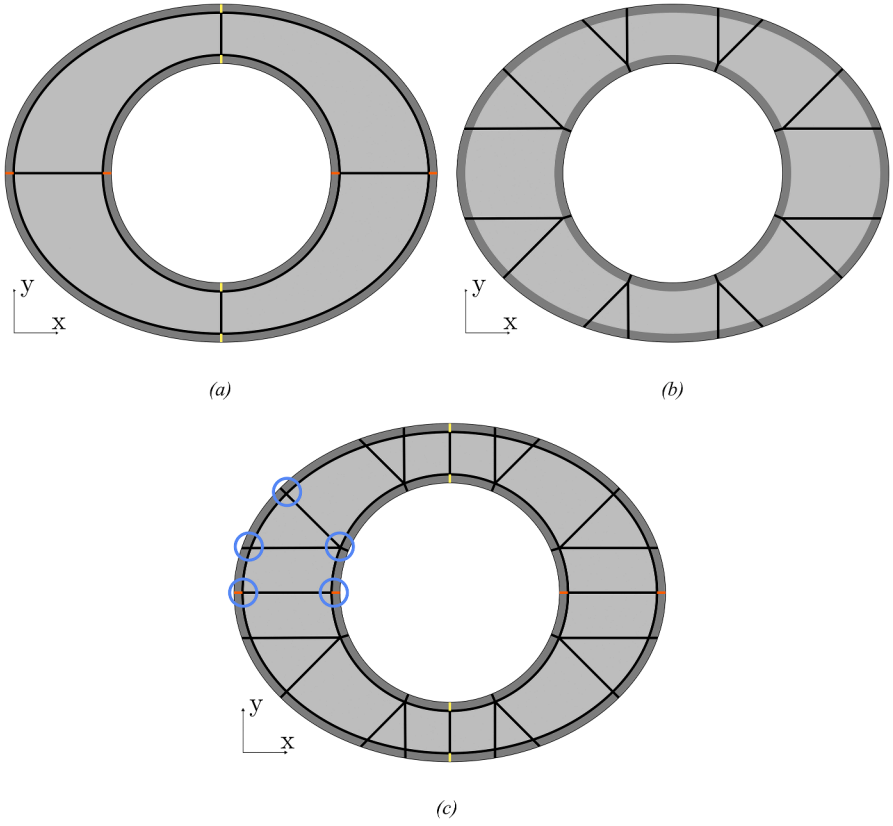

Fig. 12. Ply cuts pattern on (a) 0° layer, with black and yellow for one layer and black and orange for the other layer and on (b) 45° layer; (c) superposition of 0° and 45° layers with some butt joint overlaps highlighted (thickness not in scale).

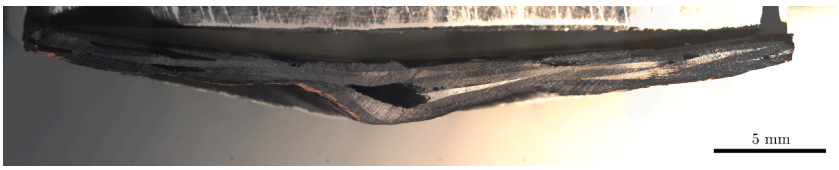

Fig. 13. Cut out section of a wrinkle with a noticeable void left due to ply separation.

The plies must be separated also over the radial direction, with the pattern illustrated in Fig. 12. This pattern required 8 patches for each ply at 0°: two rectangular patches for the region shaped as a cylinder (region A in Fig. 11), two rectangular patches for the cylindrical region with elliptical base (region C in Fig. 11) and four patches for the transition region (region B in Fig. 11), which is a section of a cone with one elliptical base and one circular base. The patches for the transition region were not perfectly aligned at 0° over the whole surface, with errors reaching about 45°. This fact was due to the cutting method of the patch that was obtained by approximating the 3D shape over a planar surface and, consequently, having perfectly aligned fibers would have required to have an ad hoc textile style following the curve. This discrepancy was not considered critical since the component was not a structural one. It should be also considered that, to reduce the orientation mismatch, one should increase the number of patches, thus obviously also increasing the separation of plies. For this reason, it was decided to give priority to the plies continuity rather than to their precise orientation. The joining point of the cylindrical regions was phased by 90° between the two 0° plies, to reduce superposition of butt joints. Fig. 12a reports the cut pattern for the layers at 0°; the first layer cuts are represented by the black and yellow lines, while the second layer cuts are in black and orange. Each ply at 45° was composed by 16 patches, 8 with rectangular shape, which were intended to provide continuity at the junction between the cylinders and the baffles, and another 8 with triangular-like shape, which were introduced to fill the remaining regions that cannot be covered by the rectangular patches, as shown in Fig. 12b. By superposing the two diagrams, the diagram of Fig. 12c can be obtained and it can be seen that the regions where all three joints are coincident are, ideally, concentrated in points placed at the transition between the cylinders and the baffles, with part of them highlighted in the sketch.

5.2. Results of the manufacturing trials and implemented corrective actions

To obtain acceptable quality in the final piece it was decided to perform some trials on smaller component. For the trials the same mold of the internal part was used, which was designed to be separable in two pieces, aiming to simplify the demolding phase, and was produced in aluminum. The first trials consisted in the production of short cylindrical sections with circular base. These trials showed the tendency of the material to create wrinkles when cured, which were localized near the junctions of the 45° ply. These wrinkles occurred only in tangential direction, due to the closed axisymmetric geometry, while in the axial direction the material did not show this behavior. A magnification of a cut out section of the wrinkle is reported in Fig. 13, where it can be seen the void that is created under the wrinkle, which can undermine the integrity of the piece.

Pre-compaction cycles during the lamination were tested while laminating the small cylinders, but this procedure was deemed unfeasible for the whole component, because of the vacuum bagging procedure complexity. The test using pre-compaction indicated that the insurgence of wrinkles was mainly driven by the 45° ply, since the wrinkle arose in the compaction after the 45° ply deposition and after manually removing the wrinkles the final component did not show any defect. To solve this issue two techniques were adopted to compensate the impossibility of pre-compaction. The first one was to completely avoid the tangential superposition of the different patches so that the layup was laminated leaving about 1 mm of space between the different patches in the tangential direction. This allowed the plies to slightly slide during the curing cycle, without possible interference between them. In the axial direction it was decided to maintain the superposition of all the patches, since the component is free to expand during the compaction. The second solution was to pre stretch the plies at 45°, thus counteracting their sliding when compacted and avoiding the wrinkles. These solutions, applied during the lamination of the internal parts, allowed to reduce the wrinkle formation leading to acceptable quality pieces, as shown in Fig. 14. The technological trials allowed to define a lamination procedure for the internal parts capable of producing pieces without wrinkles or excessive distortions.

Fig. 14. Polymeric precursor after curing.

After the precursor curing, the pieces were firstly pyrolyzed in inert atmosphere, leaving only the carbonaceous residual of the matrix and the fibers. At this stage of the process the material can be easily machined. This property was exploited to bring the part to the required dimensions and to produce the holes required for noise attenuation and for the application of bolts, rivets and floating nuts. The last step required before the infiltration is the application of the foam template. The part is then infiltrated with molten silicon obtaining the final piece, with both the C/SiC CMC and the SiSiC foam. This procedure was repeated for all the eleven parts, both internal parts and the simpler half cylinder external parts, composing the final assembly of the muffler.

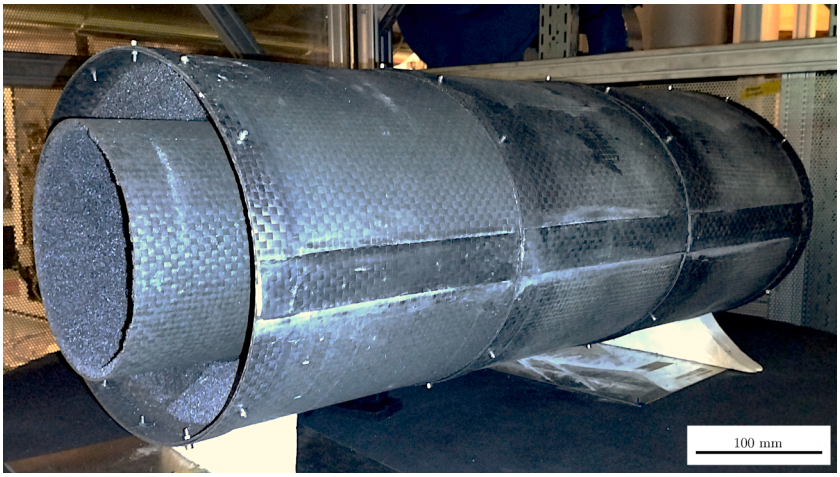

Fig. 15. Final assembled muffler.

Considering that the scope of the study was to demonstrate the technological feasibility of the muffler construction, the final assembled muffler, illustrated in Fig. 15, even if affected by some small dimensional mismatch between the parts, showed an acceptable quality and proved that this kind of structures for high temperatures applications can be produced using alternative materials to metals.

6. Conclusions

This study allowed to gain experience on the application of Ceramic Matrix Composite to secondary aeronautical structures. In particular, the study covered the redesign of the muffler into a modular configuration and, exploiting the possibility to co-infiltrate the piece and the ceramic foam, allowed to introduce a solution to increase the noise attenuation performance. The material mechanical properties were investigated, studying both the as built state and the oxidized state. The latter state was fundamental for the proposed application, in which the material is subjected to a working condition which promote active oxidation. The results proved that the material could survive in the oxidizing environment without showing a reduction of its mechanical properties. Starting from the results of the mechanical characterization campaign, a material model was implemented using Drucker Prager plasticity and was used into a detailed FEM model to simulate four representative conditions. Being the muffler a non-structural component, the loading state was considered as acceptable and the main stress driver was found to be the applied thermal loads, which led to a mismatch of thermal expansion between different regions of the muffler. Finally, the technological investigation allowed to define an effective method of lamination for the polymeric precursor, which was fundamental to prove the feasibility of production of such a complex part. The final assembly phase highlighted the fact that to obtain strict tolerances over dimensions and shapes further studies are required, since the manufacturing process, due to the chemical reaction and the high temperatures involved, induce deformation in the pieces, especially in closed shapes, which can be counteracted by purposely designing the mold for the precursor lamination. These deformations were not critical for this case, since only a demonstration of the technological feasibility was required, and the final assembled muffler showed an acceptable quality. This work was fundamental to increase the knowledge over the design methods for complex structures using CMC materials. In fact, one must consider factors such as the material microstructure and the production process when design CMC structures, since they influence the final properties of the material and of the structures. The experience gained so far poses the base to continue investigating the possibility of increasing the usage of CMC in aeronautical applications, shifting to the design of primary structures using this class of materials, in order to obtain more environmentally sustainable means of transportation.

CRediT authorship contribution statement

Marco Riva: Writing – original draft, Visualization, Software, Methodology, Investigation, Formal analysis, Data curation. **Alessandro Airoldi:** Writing – review & editing, Project administration, Methodology, Funding acquisition, Conceptualization. **Marco Morandini:** Writing – review & editing, Project administration, Methodology, Funding acquisition, Formal analysis, Conceptualization. **Rafał Żurawski:** Writing – review & editing, Supervision, Funding acquisition, Conceptualization. **Lorenzo Cavalli:** Writing – review & editing, Resources, Project administration, Methodology, Funding acquisition, Conceptualization. **Matteo Boiocchi:** Resources, Methodology, Investigation.

Declaration of competing interest

The authors declare that they have no known competing financial interests or personal relationships that could have appeared to influence the work reported in this paper.

Data availability

The data that has been used is confidential.

Acknowledgments

This project has received funding from the Clean Sky 2 Joint Undertaking (JU) under grant agreement No 101007816. The JU receives support from the European Union's Horizon 2020 research and innovation programme and the Clean Sky 2 JU members other than the Union.

References

[1] DS Lee, DW Fahey, A Skowron, MR Allen, U Burkhardt, Q Chen, et al., The contribution of global aviation to anthropogenic climate forcing for 2000 to 2018, Atmos. Environ. 244 (2021) 117834, https://doi.org/10.1016/j.atmosenv.2020.117834.

[2] S Gössling, A. Humpe, The global scale, distribution and growth of aviation: implications for climate change, Glob. Environ. Change 65 (2020) 102194, https://doi.org/10.1016/j.gloenvcha.2020.102194.

[3] SV Gudmundsson, M Cattaneo, R. Redondi, Forecasting temporal world recovery in air transport markets in the presence of large economic shocks: the case of COVID-19, J. Air. Transp. Manage 91 (2021) 102007, https://doi.org/10.1016/j.jairtraman.2020.102007.

[4] X Sun, S Wandelt, A. Zhang, A data-driven analysis of the aviation recovery from the COVID-19 pandemic, J. Air. Transp. Manage (2023) 102401, https://doi.org/10.1016/j.jairtraman.2023.102401.
[5] J Larsson, A Elofsson, T Sterner, J. Åkerman, International and national climate policies for aviation: a review, Clim. Policy. 19 (2019) 787–799, https://doi.org/10.1080/14693062.2018.1562871.
[6] U Ahmed, F Ali, I. Jennions, A review of aircraft auxiliary power unit faults, diagnostics and acoustic measurements, Prog. Aerosp. Sci. 124 (2021) 100721, https://doi.org/10.1016/j.paerosci.2021.100721.
[7] S Chivate, P Hujare, R Askhedkar, D Hujare, S. Chinchanikar, A review on acoustic performance analysis of reactive muffler, Mater. Today Proc. 63 (2022) 613–622, https://doi.org/10.1016/j.matpr.2022.04.262.
[8] W. Krenkel, Cost effective processing of cmc composites by melt infiltration (Lsi-Process), in: M Singh, T Jessen (Eds.), Ceram. Eng. Sci. Proc., Hoboken, NJ, USA 22, John Wiley & Sons, Inc., 2001, pp. 443–454, https://doi.org/10.1002/9780470294680.ch52.
[9] W Krenkel, B Heidenreich, R. Renz, C/C-SiC composites for advanced friction systems, Adv. Eng. Mater. 4 (2002) 427–436, https://doi.org/10.1002/1527-2648(20020717)4:7<427::AID-ADEM427>3.0.CO;2-C.
[10] J Schulte-Fischedick, S Seiz, N Lützenburger, A Wanner, H. Voggenreiter, The crack development on the micro- and mesoscopic scale during the pyrolysis of carbon fibre reinforced plastics to carbon/carbon composites, Compos. Part A: Appl. Sci. Manuf. 38 (2007) 2171–2181, https://doi.org/10.1016/j.compositesa.2007.06.013.
[11] J Schulte-Fischedick, A Zern, J Mayer, M Rühle, M Frieß, W Krenkel, et al., The morphology of silicon carbide in C/C–SiC composites, Mater. Sci. Eng. A 332 (2002) 146–152, https://doi.org/10.1016/S0921-5093(01)01719-1.
[12] G. Camus, Development of damage in a 2D woven C/SiC composite under mechanical loading: I. Mechanical characterization, Compos. Sci. Technol. 56 (1996) 1363–1372, https://doi.org/10.1016/S0266-3538(96)00094-2.
[13] B. Heidenreich, Melt Infiltration Process, editor, in: W Krenkel (Ed.), Ceram. Matrix Compos, Wiley-VCH Verlag GmbH & Co. KGaA, Weinheim, Germany, 2008, pp. 113–139, https://doi.org/10.1002/9783527622412.ch5.
[14] RR. Naslain, SiC-matrix composites: nonbrittle ceramics for thermo-structural application, Int. J. Appl. Ceram. Technol. 2 (2005) 75–84, https://doi.org/10.1111/j.1744-7402.2005.02009.x.
[15] Y Zhang, L Zhang, Y Liu, X Liu, B. Chen, Oxidation effects on in-plane and interlaminar shear strengths of two-dimensional carbon fiber reinforced silicon carbide composites, Carbon 98 (2016) 144–156, https://doi.org/10.1016/j.carbon.2015.10.091.
[16] F Lamouroux, G. Camus, Oxidation effects on the mechanical properties of 2D woven C/SiC composites, J. Eur. Ceram. Soc. 14 (1994) 177–188, https://doi.org/10.1016/0955-2219(94)90105-8.
[17] R. Naslain, Design, preparation and properties of non-oxide CMCs for application in engines and nuclear reactors: an overview, Compos. Sci. Technol. 64 (2004) 155–170, https://doi.org/10.1016/S0266-3538(03)00230-6.
[18] F Raether, J Meinhardt, A. Kienzle, Oxidation behaviour of carbon short fibre reinforced C/SiC composites, J. Eur. Ceram. Soc. 27 (2007) 1217–1221, https://doi.org/10.1016/j.jeurceramsoc.2006.04.019.
[19] Y Shi, K Tushtev, J-M Hausherr, D Koch, K. Rezwan, Oxidation kinetics and its impact on the strength of carbon short fiber reinforced C/SiC ceramics, Adv. Eng. Mater. 15 (2013) 19–26, https://doi.org/10.1002/adem.201200130.
[20] J Dai, J Sha, Y Zu, Z Zhang, X Zou, M. Lei, Microstructural tailoring and its influence on oxidation resistance of carbon fiber-reinforced C-SiC matrix composites, Ceram. Int. 45 (2019) 2044–2052, https://doi.org/10.1016/j.ceramint.2018.10.105.
[21] W Krenkel, F. Berndt, C/C–SiC composites for space applications and advanced friction systems, Mater. Sci. Eng. A 412 (2005) 177–181, https://doi.org/10.1016/j.msea.2005.08.204.
[22] C28 Committee. Test Method for Monotonic Tensile Behavior of Continuous Fiber-Reinforced Advanced Ceramics With Solid Rectangular Cross-Section Test Specimens at Ambient Temperature. ASTM International; n.d. https://doi.org/10.1520/C1275-15.
[23] D30 Committee. Test Method for In-Plane Shear Response of Polymer Matrix Composite Materials By Tensile Test of a 45 Laminate. ASTM International; n.d. https://doi.org/10.1520/D3518_D3518M-18.
[24] C28 Committee. Test Method for Monotonic Compressive Strength Testing of Continuous Fiber-Reinforced Advanced Ceramics With Solid Rectangular Cross-Section Test Specimens at Ambient Temperatures. ASTM International; n.d. https://doi.org/10.1520/C1358-18.
[25] S. Baste, Inelastic behaviour of ceramic-matrix composites, Compos. Sci. Technol. 61 (2001) 2285–2297, https://doi.org/10.1016/S0266-3538(01)00122-1.
[26] X Fan, X Yin, X Cao, L Chen, L Cheng, L. Zhang, Improvement of the mechanical and thermophysical properties of C/SiC composites fabricated by liquid silicon infiltration, Compos. Sci. Technol. 115 (2015) 21–27, https://doi.org/10.1016/j.compscitech.2015.04.019.
[27] E Novembre, A Airoldi, M Riva, AM Caporale, L Cavalli, Stefano De, M. Fumo, A macroscale damage model for the tensile and bending failure of C/C-SiC structural laminates, J. Eur. Ceram. Soc. (2024), https://doi.org/10.1016/j.jeurceramsoc.2024.05.072. S0955221924005077.
[28] Y Shi, F Kessel, M Friess, N Jain, K. Tushtev, Characterization and modeling of tensile properties of continuous fiber reinforced C/C-SiC composite at high temperatures, J. Eur. Ceram. Soc. 41 (2021) 3061–3071, https://doi.org/10.1016/j.jeurceramsoc.2020.09.043.
[29] P Galizia, D. Sciti, Disclosing residual thermal stresses in UHT fibre-reinforced ceramic composites and their effect on mechanical behaviour and damage evolution, Compos. Part B Eng. 248 (2023) 110369, https://doi.org/10.1016/j.compositesb.2022.110369.
[30] AM Caporale, P Galizia, B Zanardi, A Vinci, D Sciti, A. Airoldi, A bi-phasic numerical approach for non-linear response and stiffness recovery related to residual thermal stress in UHTCMCs, J. Eur. Ceram. Soc. (2024), https://doi.org/10.1016/j.jeurceramsoc.2024.03.038. S0955221924002565.
[31] A Airoldi, M Boiocchi, M Natali, C Mirani, L Di Pancrazio, G Consiglio, et al., Feasibility of a morphing rocket nozzle for thrust vector control based on corrugated composite laminates, Appl. Compos. Mater. (2022), https://doi.org/10.1007/s10443-022-10082-9.
[32] M Riva, A Airoldi, T Turconi, P Ballarin, M Boiocchi, L. Bottasso, Development and manufacturing of flexible joints based on corrugated composite laminates, Compos. Struct. 308 (2023) 116683, https://doi.org/10.1016/j.compstruct.2023.116683.
[33] ABAQUS/Standard User's Manual, Version 6.14. Dassault Systèmes Simulia Corp.; n.d.
[34] S Flores, AG Evans, FW Zok, M Genet, B Cox, D Marshall, et al., Treating matrix nonlinearity in the binary model formulation for 3D ceramic composite structures, Compos. Part Appl. Sci. Manuf. 41 (2010) 222–229, https://doi.org/10.1016/j.compositesa.2009.10.020.
[35] HJ Lim, H Choi, MJ Lee, GJ. Yun, An efficient multi-scale model for needle-punched Cf/SiCm composite materials with experimental validation, Compos. Part B Eng. 217 (2021) 108890, https://doi.org/10.1016/j.compositesb.2021.108890.